Physics of Electron Cyclotron Current Drive on DIII–D

C.C. Petty,[1] R. Prater,[1] T.C. Luce,[1] R.A. Ellis,[2] R.W. Harvey,[3] J.E. Kinsey,[4] L.L. Lao,[1] J. Lohr,[1] M.A. Makowski,[5] and K.-L. Wong[2]

[1]General Atomics, P.O. Box 85608, San Diego, California 92186-5608
 email: leonard@fusion.gat.com
[2]Princeton Plasma Physics Laboratory, Princeton, New Jersey 08543
[3]CompX, Del Mar, California
[4]Lehigh University, Bethelehem, Pennsylvania
[5]Lawrence Livermore National Laboratory, P.O. Box 808, Livermore, California 94551

Abstract. Recent experiments on the DIII-D tokamak have focused on determining the effect of trapped particles on the electron cyclotron current drive (ECCD) efficiency. The measured ECCD efficiency increases as the deposition location is moved towards the inboard midplane or towards smaller minor radius for both co and counter injection. The measured ECCD efficiency also increases with increasing electron density and/or temperature. The experimental ECCD is compared to both the linear theory (Toray-GA) as well as a quasilinear Fokker-Planck model (CQL3D). The experimental ECCD is found to be in better agreement with the more complete Fokker-Planck calculation, especially for cases of high rf power density and/or loop voltage.

1. Introduction

Electron cyclotron current drive (ECCD) experiments on the DIII-D tokamak are solidifying the physics basis for localized, off-axis current drive, the goal being to validate a predictive model for ECCD [1,2]. Using internal magnetic measurements from motional Stark effect (MSE) polarimetry [3,4], driven currents as small at 1% of the total plasma current can be accurately measured. As a result, the physics of ECCD can be explored in unprecedented detail since the ECCD efficiency can be determined over a wide range of plasma conditions. This is a significant advance over previous ECCD studies on tokamaks and stellarators that mainly measured the magnitude of the driven current from the change in the loop voltage at the plasma surface required to maintain a constant plasma current [5,6].

Electron cyclotron current drive results from the selective heating of electrons traveling in one toroidal direction to decrease their collision frequency, and thus increase their contribution to the toroidal current compared to their unheated counterparts moving in the opposite direction [7,8]. This current drive mechanism is offset by the mirror trapping of electrons in toroidal geometry that drives current in the reverse direction [9]. The opposition between these two current drive mechanisms makes it imperative to study the influence of electron trapping on ECCD, which is done in this paper by determining the current drive dependences as a function of the poloidal deposition location, normalized radius of deposition, and electron beta. The electron trapping effects on the ECCD are measured for both co and counter injection.

The measured ECCD dependences on electron trapping are compared with the theoretical dependences calculated by a bounce-averaged, quasilinear Fokker-Planck model [10], including the effect of the residual parallel electric field ($E_{\parallel}$), which is the most complete model of ECCD available to us. These experiments satisfy all of the underlying theoretical assumptions, such as full absorption of the wave energy before the cold plasma resonance is reached and good confinement of the heated electrons. This paper also compares the experimental ECCD to the theoretical current drive in the $E_{\parallel} = 0$, low power density limit as determined from the linearized Fokker-Planck equation using ray tracing codes [11,12,13,14]. While the linear ECCD efficiency is not expected to accurately predict the experimental results in general, it may be an appropriate approximation in some regimes.

2. Experimental Setup

These ECCD experiments are done on the DIII-D tokamak [15], typical parameters for which are major radius $R = 1.7$ m, minor radius $a = 0.6$ m, elongation $\kappa = 1.8$, toroidal magnetic field strength $B_T = 1.65$–2.15 T, and plasma current $I_p = 0.6$–1.3 MA. The working gas for

plasma fueling and neutral beam injection is deuterium. These experiments use up to five gyrotron oscillators operating at 110 GHz, with a maximum combined power of $P_{ec} = 2.3$ MW injected into the plasma [16,17,18]. The beams from the gyrotrons are launched into the tokamak from the low magnetic field side using a pair of mirrors that allows the poloidal aiming to be changed between plasma pulses. Several gyrotrons are connected to launchers that allow the user to switch between co and counter injection for maximum experimental flexibility. The polarization corresponding to the X-mode dispersion relation is launched in these experiments since it is absorbed strongly near the second harmonic of the electron cyclotron resonance. The polarization, propagation, and deposition of the launched electron cyclotron waves have been confirmed experimentally on DIII-D [19,20,21].

Two separate methods are used on DIII-D to deduce the ECCD from the MSE signals. In the first method, the noninductive current drive is determined from the evolution of the poloidal magnetic flux obtained from a magnetic equilibrium reconstruction constrained by the MSE data [22,23]. The first localized measurements of the ECCD profile were made using this analysis method on DIII-D [24,25]. In the second method, the measured MSE signals are compared to simulations of the MSE evolution using a model of the ECCD profile [1]. The parameters of the model — location, width, and magnitude — are adjusted until a best fit between the measured and simulated MSE signals is obtained. Although the two analysis methods have different strengths and weaknesses [1], they give similar results when compared using standard test cases. In this paper, the ECCD results are obtained using the second method exclusively, which has the advantage that arbitrarily narrow current drive profiles can be handled by the direct fits to the raw MSE data.

3. Effect of Electron Trapping on ECCD

The experiments discussed in this section vary the interaction between the electron cyclotron waves and the particles in both velocity space and real space, and primarily test the effect of electron trapping on the ECCD efficiency. Since many of these experiments vary the electron density (n_e) and temperature (T_e), it is convenient to normalize out the usual power per particle and collisionality effects when discussing the current drive efficiency, resulting in a dimensionless ECCD efficiency given by

$$\varsigma_{ec} = \frac{e^3}{\varepsilon_0^2} \frac{I_{ec} R n_e}{P_{ec} k T_e} = 3.27 \frac{I_{ec}(\text{A}) R(\text{m}) n_{19}}{P_{ec}(\text{W}) T_e(\text{keV})} \quad , \tag{1}$$

where R is the average major radius of the plasma surface, n_{19} is the electron density in units of 10^{19} m^{-3}, e is the charge of an electron, ε_0 is the permittivity of free space, and k is the Boltzmann constant. The normalization given in Eq. (1) with density and temperature is appropriate for central current drive; however, when electron trapping effects are strong, there are additional n_e and T_e dependences as discussed later in this section. The main tenets of electron trapping theory are examined by determining the ECCD efficiency as a function of the poloidal deposition location (θ_{pol}), normalized radius of deposition (ρ), and electron beta (β_e). Here the poloidal angle is defined to be 0 deg on the outboard midplane, 90 deg at the top of the plasma, and 180 deg on the inboard midplane. Note that the measured ECCD reported in this paper necessarily includes the synergistic current drive that is proportional to both the loop voltage and the ECCD power. Theoretically, the residual loop voltage primarily affects the non-Maxwellian resistivity, resulting in a distorted electron distribution function that leads to a small but measurable modification in the ECCD.

Varying the parallel index of refraction ($N_\parallel$) allows the electron trapping effects to be determined for co and counter ECCD separately and tests the velocity space interaction betwen electron cyclotron waves and electrons. Figure 1 shows that scanning $N_\parallel$ from positive to negative values at the point of absorption switches the ECCD from the co to the counter direction, with radial injection ($N_\parallel = 0$) driving little current. The value of $N_\parallel$ is varied by changing the toroidal injection angle on a shot-to-shot basis. Theoretically, the ECCD efficiency is expected to increase with a larger magnitude of $N_\parallel$ since the electron cyclotron waves interact with higher parallel velocity electrons. (However, at too high an $N_\parallel$ value there

are not enough high energy electrons to damp the waves and this effect diminishes.) In Fig. 1, the measured ζ_{ec} at fixed deposition location (ρ, θ_{pol}) and fixed β_e is seen to increase with larger $|N_\parallel|$ for both co and counter injection, in agreement with the theoretical value of ζ_{ec} determined by the CQL3D quasilinear Fokker-Planck code [10], including the effect of $E_\parallel$. In this paper, the $E_\parallel$ profile used in the CQL3D modeling is determined from a loop voltage profile analysis [22]. Note in Fig. 1 that for the same $N_\parallel$ magnitude, $|\zeta_{ec}|$ is typically larger for co injection than for counter injection owing to the $E_\parallel$ effect.

The effect of electron trapping on the dimensionless ECCD efficiency is investigated by varying the poloidal location of the ECCD deposition at constant minor radius. This is effective because the local trapped particle fraction varies from small near the high field side midplane $(\theta_{pol} = 180°)$ to maximum at the low field side midplane $(\theta_{pol} = 0°)$. Figure 2 shows that the measured ζ_{ec} increases as the poloidal location of deposition is moved towards the high field side at fixed ρ and $N_\parallel$. (The maximum B_T of 2.16 T on DIII-D limits the minimum value of θ_{pol} to be ≈ 60 deg for off-axis deposition.) This effect is especially apparent in low β_e plasmas, while the θ_{pol} dependence for high β_e plasmas is weaker due to the reduced trapping effect at high electron density and temperature, as discussed later in this section. In addition, the θ_{pol} dependence of ζ_{ec} is stronger at larger ρ. The experimental data in Fig. 2 are in agreement with the θ_{pol} dependence predicted by the CQL3D code, including the effect of $E_\parallel$, for both co and counter injection. Therefore, it is easiest to drive current off-axis when the ECCD location is on the inboard side of the plasma, but at high β_e the difference between the inboard midplane and the top of the plasma is small.
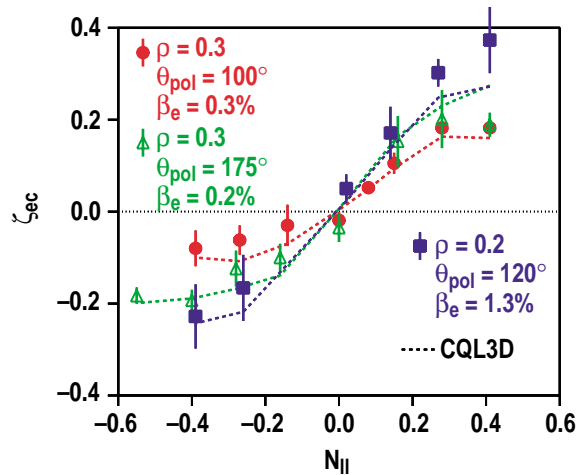

Fig. 1. Experimental dimensionless ECCD efficiency for scans of the parallel index of refraction. The normalized radius and poloidal angle of deposition, and the local electron beta are noted for each scan. The theoretical dependence from the CQL3D code is also shown (dashed lines).
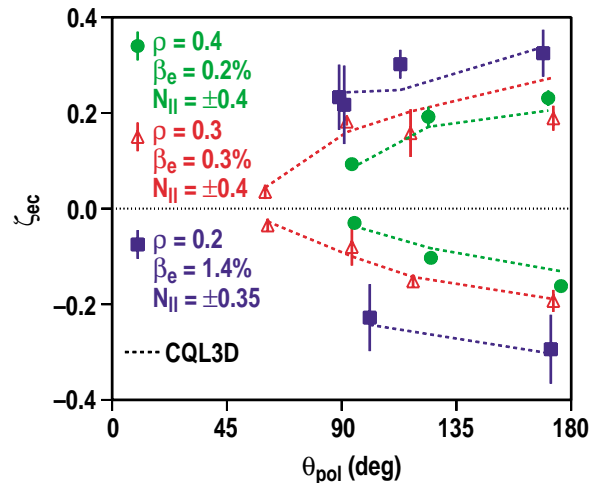
Fig. 2. Experimental dependence of the dimensionless ECCD efficiency on the poloidal angle of deposition, where positive values denote co current drive. The theoretical dependence calculated by the CQL3D code is also shown (dashed lines).

Another effect of electron trapping is that the ECCD efficiency should decrease with increasing minor radius because the trapped particle fraction increases with increasing ρ. Figure 3 shows that for low beta L-mode plasmas $(\beta_e = 0.4\%)$, the measured ζ_{ec} does decrease rapidly with increasing ρ, in agreement with the theoretical prediction from the CQL3D code. This scan is done at fixed B_T by varying the poloidal steering of the antenna while adjusting the toroidal steering to hold $N_\parallel$ fixed. The poloidal deposition location for $B_T = 2.0$ T is above the plasma axis $(\theta_{pol} = 95$ deg), where the trapped electron fraction is moderately large. This decrease in ζ_{ec} with ρ extrapolates to nearly zero current drive efficiency at $\rho \approx 0.5$ in these low beta plasmas. This would be a disappointing outcome for advanced tokamak (AT) scenarios, where the ECCD needs to be located near $\rho \approx 0.5$ for current profile control [26,27]. Fortunately, Fig. 3 shows that for high beta H-mode plasmas $(\beta_e = 1.9\%)$ at the same magnetic field strength, the measured ζ_{ec} decreases little with increasing ρ. This is explained theoretically [28] by the shift in the electron cyclotron resonance to higher parallel velocities

owing to the stronger damping of electron cyclotron waves at higher electron density and/or temperature as well as relativistic effects. This increases the separation in velocity space between the position of the power deposition on the electron cyclotron resonance curve and the trapped-passing boundary, making the current carrying electrons less likely to pitch angle scatter into the trapped region which increases the current drive efficiency. In addition to the reduced trapping effects, the interaction of electron cyclotron waves with more energetic electrons (owing to the stronger damping) can also lead to an additional increase in the current drive efficiency at higher n_e and T_e. The theoretical ECCD efficiency from the CQL3D code, including the effect of $E_{||}$, is in agreement with the experiment for both the strong trapping and weak trapping situations in Fig. 3. Thus, the theoretical prediction of an ECCD efficiency of $\zeta_{ec} \approx 0.2$ at $\rho = 0.5$ in future AT scenarios [26,27] with $\langle\beta\rangle$ up to 7.5% appears to be achievable experimentally on DIII-D, which should be sufficient to sustain hollow current profiles.

The role that reduced trapping effects play in increasing the ECCD efficiency is confirmed by the radial scan at $B_T = 1.8$ T in high beta H-mode plasmas ($\beta_e = 1.6\%$) that is also shown in Fig. 3. The reduced magnetic field strength moves the deposition to the high field side ($\theta_{pol} = 160$ deg) where the trapped particle fraction is lower, resulting in higher measured values of ζ_{ec} that decrease relatively slowly with increasing ρ in agreement with the prediction of the CQL3D code. When the ECCD location is moved to the inboard midplane, the trapped-passing boundary and electron cyclotron resonance curve are shifted as far apart as possible in velocity space; therefore, the favorable beta dependence of ζ_{ec} is expected to become less apparent. This is confirmed experimentally in Fig. 4, where radial scans of the measured ECCD efficiency for co and counter injection near $\theta_{pol} = 180$ deg are plotted for both H-mode and L-mode plasmas. For these scans, the radius of deposition is varied by changing B_T while the poloidal steering of the antenna is adjusted to keep the deposition near the inboard midplane. In addition, the toroidal steering of the antenna is adjusted to keep $N_{||}$ fixed at ±0.35. The gradual reduction in ζ_{ec} with increasing ρ for both co and counter ECCD indicates that the effects of electron trapping are reduced for deposition on the inboard midplane. In the region around $0.3 < \rho < 0.4$, an increase in the plasma beta from 0.4% to 1.5% hardly changes the measured value of ζ_{ec}. This is in agreement with the CQL3D code, including the effect of $E_{||}$, which predicts that the theoretical ECCD efficiency should change by only ≈10% between these two beta values at this deposition location.

4. Comparison of Linear and Fokker-Planck Models

The goal of these ECCD experiments is to validate a predictive model of ECCD, with the quasilinear Fokker-Planck code CQL3D [10] representing the most complete model of ECCD
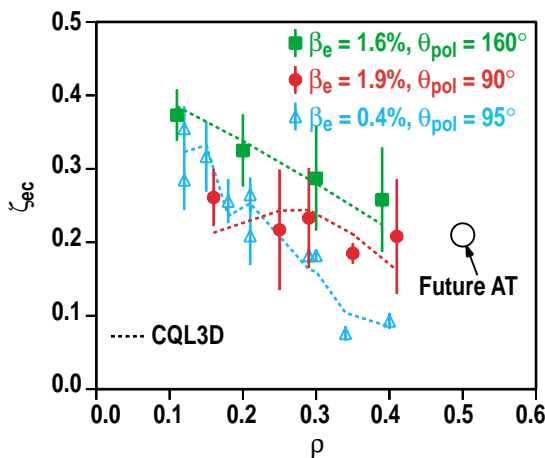

Fig. 3. Experimental dimensionless ECCD efficiency for co injection for scans of the normalized radius of deposition in low beta L-mode and high beta H-mode plasmas. The theoretical dependence calculated by the CQL3D code is also shown (dashed lines).
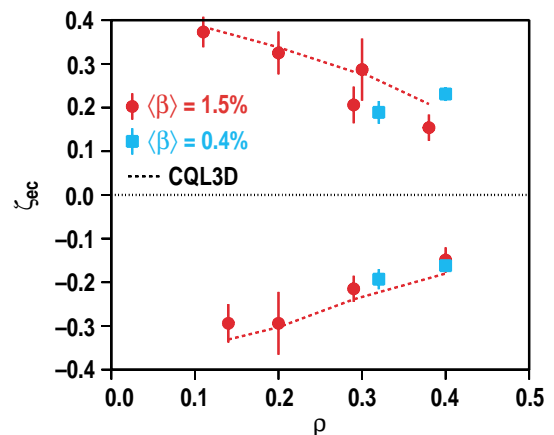
Fig. 4. Measured dimensionless ECCD efficiency for scans of the normalized radius of deposition on the inboard midplane for low beta L-mode and high beta H-mode plasmas. Positive values denote co current drive. The theoretical dependence calculated by the CQL3D code is shown (dashed lines).

that is available to us. The experimental data presented in Section 3 show that the measured ECCD on DIII-D is in good agreement with the CQL3D code, including the effect of $E_{||}$, for both co and counter injection over a wide range of conditions. However, since it is also a common practice to calculate the theoretical ECCD from the relativistic, linearized Fokker-Planck equation using ray tracing codes [11,12,13,14], it is worthwhile to make a detailed comparison between the experimental data and both the linear model and quasilinear Fokker-Planck model. It is especially important to determine if the physics improvements in the more complete Fokker-Planck model (*i.e.,* d.c. parallel electric field, rf quasilinear diffusion, momentum conservation in electron-electron collisions) actually bring theory and experiment into better agreement or not.

First, if the effect of the parallel electric field is neglected in the CQL3D calculation, then the agreement between theory and experiment declines for co injection. Figure 5 shows the ratio of the measured and theoretical co ECCD as a function of the measured $E_{||}$ normalized to the critical field (E_{cr}) [29] for runaway of thermal electrons at the ECCD location. In Fig. 5, $E_{||}$ is defined to be the measured value of the flux-surface-average loop voltage at the ECCD deposition location divided by $2\pi R$, where the loop voltage profile is determined from the evolution of the poloidal magnetic flux [22]. A statistical comparison between the CQL3D model with $E_{||} = 0$ and the measured ECCD for the dataset in Fig. 5 yields a reduced χ^2 of 1.8, which is significantly larger than the reduced χ^2 of 1.0 for the comparison where $E_{||}$ is retained in the CQL3D modeling. There is some uncertainty in the injected ECCD power that is not included in the error bars in Fig. 5, but the statistical comparison over a large number of points reduces the effect of this problem. Figure 5 also shows that the inclusion of the parallel electric field in the theory most affects the cases that have large values of $E_{||}/E_{cr}$, as expected.

Second, if the linear ECCD efficiency calculated by the Toray-GA code is used, then the agreement between theory and experiment declines for co injection. Figure 6 shows the ratio of the measured and theoretical co ECCD as a function of the rf power density (Q_{ec}) normalized to the square of the electron density at the ECCD location. The main differences between the two theoretical models in Fig. 6 are the neglect in Toray-GA of nonthermal effects as well as the neglect in Toray-GA of momentum conservation in electron-electron collisions. A statistical comparison between Toray-GA and the measured ECCD for the dataset in Fig. 6 gives a reduced χ^2 of 6.4, which is larger than the reduced χ^2 of 1.8 for the CQL3D model with $E_{||}$ set to zero (to be consistent with the neglect of $E_{||}$ in the linear theory). Theoretically, the ECCD efficiency is expected to be power dependent at high
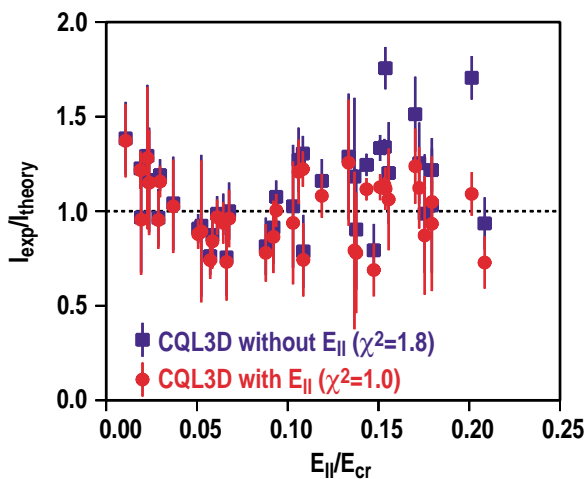

Fig. 5. Ratio of measured and theoretical ECCD as a function of the d.c. parallel electric field normalized to the critical field. The theoretical ECCD is calculated by the CQL3D code with and without including the effect of $E_{||}$.
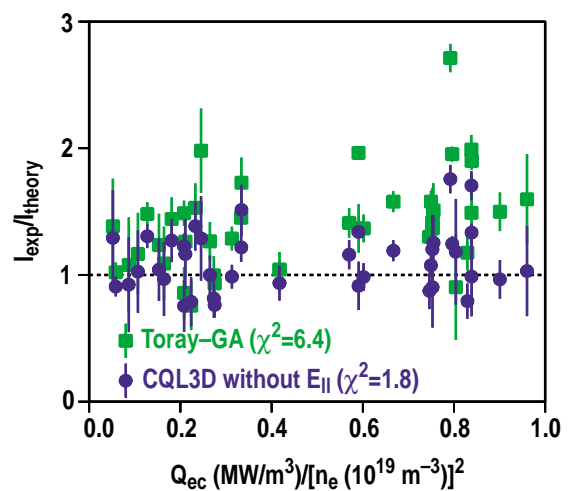
Fig. 6. Ratio of measured and theoretical ECCD as a function of the relative rf power density. The theoretical ECCD is calculated by the linear Toray-GA code and the quasilinear CQL3D code (not including the effect of $E_{||}$).

rf power densities [30], *i.e.*, Q_{ec} (MW/m^3) ≥ 0.5 $[n_e (10^{19}$ m$^{-3})]^2$. Figure 6 clearly shows that the largest discrepancies between the Toray-GA code and experiment occur for rf power densities above this level. However, the linear theory also slightly underpredicts the measured co ECCD by $\approx 15\%$ (relative to CQL3D) even for low values of Q_{rf}. This is mostly explained by the neglect of momentum conservation in electron-electron collisions in Toray-GA, which is calculated to be a 10% effect by CQL3D, although this is not the only difference between these two codes in this limit. While the linear theory is a relatively good predictor of co ECCD for low rf power densities (and presumably low loop voltages), it is also interesting to note that for counter injection both Toray-GA and CQL3D agree with the measured ECCD equally well. This appears to be a fortuitous result for the linear theory because the neglect of nonthermal effects and momentum conservation in Toray-GA, which underestimates the ECCD magnitude, tends to offset the neglect of $E_{\parallel}$, which overestimates the ECCD magnitude for counter injection. Nevertheless, taking the whole ECCD dataset on DIII–D into account, the more complete quasilinear Fokker-Planck theory of ECCD, including the effect of $E_{\parallel}$, is clearly the better predictor of the experimental ECCD efficiency.

5. Conclusions

Recent experiments on the DIII-D tokamak have made great progress in validating a predictive model of ECCD, especially in regard to the effects of electron trapping. The measured ECCD switches from the co to the counter direction as the toroidal injection angle is varied, with radial injection driving little current. The current drive efficiency for both co and counter ECCD is measured to increase as the poloidal location of deposition is moved from the low field side to the high field side of the machine, which is expected since the local trapped electron fraction is lower near the inboard midplane. In low beta plasmas, the experimental ECCD efficiency decreases rapidly as the deposition is moved off-axis towards the top of the machine, but this radial dependence becomes much weaker in high beta plasmas. Thus, the detrimental effects of electron trapping on the ECCD efficiency are greatly diminished at high electron density and/or temperature. Owing to this favorable density/temperature dependence, high ECCD efficiencies are expected in future high beta advanced tokamak plasmas. The measured ECCD is in good agreement with the CQL3D quasilinear Fokker-Planck code, including the effect of the residual parallel electric field, over a wide range of conditions. Although the differences in the theoretical ECCD calculated by the CQL3D code and linear theory are small at low rf power densities and low parallel electric fields, the experimental data clearly show that the more complete quasilinear Fokker-Planck modeling is required to obtain good agreement with measurements at high rf power densities and/or high parallel electric fields.

Acknowledgment

References

[1]   C.C. Petty, *et al.,* Nucl. Fusion **41**, 551 (2001).
[2]   C.C. Petty, *et al.,* "Detailed Measurements of the Electron Cyclotron Current Drive Efficiency on DIII-D," submitted to Nucl. Fusion.
[3]   F.M. Levinton, *et al.,* Phys. Rev. Lett. **63**, 2060 (1989).
[4]   B.W. Rice, K.H. Burrell, L.L. Lao, Y.R. Lin-Liu, Phys. Rev. Lett. **79**, 2694 (1997).
[5]   V. Erckmann, V. Gasparino, Plasma Phys. Control. Fusion **36**, 1869 (1994).
[6]   B. Lloyd, Plasma Phys. Control. Fusion **40**, A119 (1998).
[7]   N.J. Fisch, A.H. Boozer, Phys. Rev. Lett. **45**, 720 (1980).
[8]   N.J. Fisch, Rev. Mod. Phys. **59**, 175 (1987).
[9]   T. Ohkawa, "Steady-State Operation of Tokamaks by rf Heating," General Atomics Report GA-A13847 (1976).
[10]   R.W. Harvey, M.G. McCoy, in Proc. of the IAEA Technical Committee Meeting, Montreal, 1992 (IAEA, Vienna, 1993) 498.

[11]   A.H. Kritz, H. Hsuan, R.C. Goldfinger, D.B. Batchelor, in Proc. of the 3rd Int. Symposium on Heating in Toroidal Plasmas, Grenoble, 1982, Vol. II (Brussels, CEC) p. 707.

[12]   R.H. Cohen, Phys. Fluids **30**, 2442 (1987).

[13]   K. Matsuda, IEEE Trans. Plasma Sci. **17**, 6 (1989).

[14]   Y.R. Lin-Liu, *et al.*, Controlled Fusion and Plasma Physics (Proc. 26th Euro. Conf., Maastricht, 1999), Vol. 23J (European Physical Society, Geneva, 1999) p 1245.

[15]   J.L. Luxon, Nucl. Fusion **42**, 614 (2002).

[16]   R.W. Callis, *et al.*, Fusion Technol. (Proc. 20th Symp. Marseille, 1998), Vol. 1, Association EURATOM-CEA, Saint-Paul-Lez-Durance (1998) 315.

[17]   J. Lohr, *et al.*, Infrared and Millimeter Waves (Proc. 23rd Int. Conf., Colchester, 1998), University of Essex, Colchester (1998) 269.

[18]   J. Lohr, *et al.*, Radiofrequency Power in Plasmas (Proc. 14th Int. Conf., Oxnard, 2001), AIP, New York (2001) 314.

[19]   C.C. Petty, *et al.*, Radiofrequency Power in Plasmas (Proc. 13th Int. Conf., Annapolis, 1999), AIP, New York (1999) 245.

[20]   C.C. Petty, *et al.*, Strong Microwaves in Plasmas (Proc. 4th Int. Conf., Nizhny Novgorod, 1999), Vol. 1, Russian Academy of Sciences, Nizhny Novgorod (2000) 41.

[21]   C.C. Petty, *et al.*, Radiofrequency Power in Plasmas (Proc. 14th Int. Conf., Oxnard, 2001), AIP, New York (2001) 275.

[22]   C.B. Forest, *et al.*, Phys. Rev. Lett. **73**, 2444 (1994).

[23]   L.L. Lao, *et al.*, Radiofrequency Power in Plasmas (Proc. 14th Int. Conf. Oxnard, 2001), AIP, New York (2001) 310.

[24]   T.C. Luce, *et al.*, Phys. Rev. Lett. **83**, 4550 (1999).

[25]   T.C. Luce, *et al.*, Plasma Phys. and Control. Fusion **41** B119 (1999).

[26]   H.E. St. John, T.S. Taylor, Y.R. Lin-Liu, A.D. Turnbull, Plasma Physics and Controlled Nuclear Fusion Research 1994 (Proc. 15th Int. Conf., Seville, 1994), Vol. 3 (IAEA, Vienna, 1996) p. 603.

[27]   A.D. Turnbull, T.S. Taylor, Y.R. Lin-Liu, H.E. St. John, Phys. Rev. Lett. **74**, 718 (1995).

[28]   R. Prater, R.W. Harvey, Y.R. Lin-Liu, T.C. Luce, C.C. Petty, Radiofrequency Power in Plasmas (Proc. 14th Int. Conf., Oxnard, 2001), AIP, New York (2001) 302.

[29]   H. Knoepfel, D.A. Spang, Nucl. Fusion **19**, 785 (1979).

[30]   R.W. Harvey, M.G. McCoy, G.D. Kerbel, Phys. Rev. Lett. **62**, 426 (1989).